Soft Matter

PAPER

View Article Online
View Journal

Cite this: DOI: 10.1039/c3sm53123f

Defined 2-D microtissues on soft elastomeric silicone rubber using lift-off epoxy-membranes for biomechanical analyses

Nico Hampe, Thorsten Jonas, Benjamin Wolters, Nils Hersch, Bernd Hoffmann* and Rudolf Merkel

Surface patterning with complex molecules has become a valuable tool in cell biology and biotechnology, as it enables one to control cell shape and function in culture. However, this technique for micro-contact printing is normally performed on rigid substrates, *e.g.* Petri dishes or glass. Despite the fact that these substrates can easily be patterned they are artificially stiff environments for cells affecting their morphology and function. Those artifacts can be avoided on tissue elasticity resembling substrates, leading to a nature like cell morphology and behavior. However, reproducible patterning of very soft elastomeric substrates is challenging. Here, we describe a simple and highly accurate method through cavities of lift-off membranes for protein patterning of silicone rubber substrates in an elasticity range down to 1.5 kPa without altering their mechanical properties. Membranes are made of epoxy resin with feature sizes that can be chosen almost arbitrarily including widths down to 5 μm and aspect ratios of 100 and more. Different feature shapes were used to actively manipulate cell adhesion, cell morphology and the actin cytoskeleton on soft substrates. Manipulation of cytoskeletal organization furthermore allowed the comparison of myofibril alignment and cellular forces of cardiac myocytes. These data could show that cell forces are largely unaffected upon active disordering of overall myofibril alignment on a single cell level while aligned multicellular systems generate cell forces in an additive manner.

Received 16th December 2013
Accepted 13th January 2014

DOI: 10.1039/c3sm53123f

www.rsc.org/softmatter

Introduction

The technique of micro-contact printing (μCP), used to date for a wide spectrum of scientific applications including biological ones, was first introduced by A. Kumar and G. M. Whitesides in 1993.[1] They printed so called self-assembled monolayers (SAMs) onto gold surfaces using a stamp composed of a silicone elastomer (crosslinked polydimethylsiloxane: PDMS, Sylard 184, Dow Corning). Over the last two decades this micro-patterning technique enabled the production of geometrically defined patterns to investigate different aspects of cell behavior, *e.g.* cell spreading and adhesion formation,[2] apoptosis,[3] differentiation, migration,[4] cell growth and proliferation.[3,5,6] In the late 1990s Chen *et al.* highlighted the importance of the cell shape for cell fate. He and his colleagues compared cells on patterned and non-patterned substrates, showing that cells seeded on non-patterned substrates would not undergo apoptosis while 20% of seeded cells underwent programmed cell death on circular shaped patterned substrates. In a further experiment they decreased the diameter of the circular features from 20 μm to 10 μm resulting in an increase of apoptotic cells.[3,5] Regarding the differentiation behavior of cells it could be shown that mesenchymal stem cells (MSCs) seeded on micropatterned substrates initially form multicellular aggregates. Subsequently, patterns are able to direct lineage specification by virtue of the pattern geometry and of the cell position within the multicellular aggregates.[7] μCP has also been exploited to gain a deeper understanding of the mechanisms of cell migration. In a recent study μCP was used to print substrate-bound molecular gradients to investigate neurite outgrowth and axon guidance of single multipolar neurons.[8]

Effects on cell shape, intracellular organization and cell function have been impressively demonstrated on cardiac myocytes. Here, freshly isolated myocytes usually become pleomorphic when cultured on fibronectin (FN) coated unstructured, stiff cell culture substrates. In those cells, sarcomeres are located primarily in the cell center and artificial stress fibers connect barely ordered myofibrils at both ends to focal adhesion like adhesion spots.[4,9–11] By providing cardiac myocytes with microstructured substrates displaying adhesive features of various shapes and sizes myofibril organization, sarcomere localization as well as calcium metabolism and even contractile behavior could be tuned.[12]

An alternative strategy for generating protein patterns on the micron scale is the use of elastomeric lift-off membranes by spin-coating a silicone rubber prepolymer onto a "master"

Institute of Complex Systems, ICS-7: Biomechanics, Forschungszentrum Jülich GmbH, 52425 Jülich, Germany. E-mail: b.hoffmann@fz-juelich.de; Fax: +49 (0)2461 61 3907; Tel: +49 (0)2461 61 6734

consisting of photoresist features on a silicon wafer and subsequent prepolymer crosslinking.[13,14] However, in both cases soft and therefore sticky silicone rubber lift-off membranes were fabricated that could be used for microstructuring of stiff surfaces only.

Another elegant strategy for generating lift-off membranes is the process of micromolding in capillaries (MIMIC).[15,16] In essence the lift-off membranes are thin (approximately 25 μm) films of for example cured epoxy resin exhibiting micron-sized holes. Production of such microstencils starts with suitably shaped molds fabricated from rigid silicone elastomers by standard replica molding. Such a mold is then placed on top of a flat and rigid substrate. Subsequently, the shallow gap between the mold and the substrate is filled with the epoxy resin *via* capillary suction. Finally, the resin is cured to form a membrane and freed from the support by physical or chemical treatment.

The most crucial step in this procedure is filling the mold with the resin without trapping air bubbles or other defects. This is basically a problem of microfluidic two-phase flow, *i.e.* air and resin. The simplest experiment in this field is capillary filling. Despite its deceiving simplicity in everyday laboratory work, almost one century of scientific research on capillary filling[17–21] has resulted in a surprisingly complex picture demonstrating that void free filling of a complicated microstructure requires a delicate tuning of flows and driving forces (for details see also Experimental: Theoretical considerations). In cell biology, microstencils were used to coat the underlying stiff substrates without the need for an intermediate carrier of the protein (*e.g.* silicone rubber stamps) or to pattern cells on plastic and glass surfaces directly within the physical constrains provided by the holes of the membranes.[14]

Beyond cell shape definition substrate elasticity has been shown to be a potent cue to direct cell morphology, protein expression and differentiation enabling a closer approach to nature-like cell behavior in culture.[22–25] For most cell types substrate stiffness resembling those in native tissues (*e.g.* about 10 kPa for myocard) is most favorable. Surprisingly, substrate patterning for cell biology is often performed on very stiff substrates such as Petri dishes, glass and gold surfaces or rigid silicone rubber substrates with an elasticity (E) clearly exceeding 1 MPa.[9,26–28] As a consequence, those substrates still display an artificial environment for cells affecting their morphology and behavior. Thus, there is a need for techniques to produce microstructures on very soft elastomeric substrates without altering the mechanical properties of the soft elastomer.

Two main and complementary groups of soft, elastomeric substrates are known for generation of planar cell culture systems, *i.e.* hydrogels with clear advantages for generation of substrate elasticities below 1 kPa and systems based on cross-linked silicone oils characterized by extraordinary shelf lives and simple protein coating. Especially for hydrogels various molecules can be used for fabrication as *e.g.* alginates, PEG or cross-linked acrylamide.[22,29–31] However, micropatterning with proteins of those hydrogels typically depends either on complex chemical surface activation procedures[32–34] or on μ-contact printing techniques.[35] Unfortunately, μ-contact printing can go along with highly inhomogeneous concentrations of transferred proteins or peptides and incomplete shape reproduction. Recent developments reduced the number and complexity of chemical surface procedures for coating by deep UV-patterning of polyacrylamide substrates and subsequent simple EDC–NHS protein coupling (Tseng *et al.* 2011). Also transfer of activated proteins that physisorbed to μ-contact stamps from solution led to the formation of defined and relatively homogeneous adhesion areas on polyacrylamide gels (Rape *et al.* 2011). Both latter techniques were performed on substrate elasticities in the 6 to 8 kPa range.

On silicone rubber, as a second elastomeric system vitally necessary for biomechanical applications, surface activation can be omitted upon protein transfer due to sufficiently high physicochemical interactions between the substrate and the transferred molecule. Still, μ-contact printing leads to similarly inhomogeneous protein transfer. Moreover, extremely strong adhesion between ultrasoft rubber substrates and stamps renders μ-contact printing impossible. Finally, UV-light or plasma used to reduce surface stickiness or to further elevate protein adhesion stiffens silicone rubber surfaces in a hardly controllable manner[36,37] and therefore needs to be omitted for most biomechanical analyses.

In this article we introduce a simple patterning technique able to produce 2-D microtissues of defined shape and size on very soft elastomeric silicone-rubber substrates using novel lift-off epoxy membranes. Feature sizes and aspect ratios can be tuned in a wide range allowing the generation of patterns even on substrate elasticities as soft as 1.5 kPa. Since patterning takes place by protein physisorption and not stamping, protein denaturation is minimized and features are homogeneously coated. The technique allows the simultaneous analysis of cell/colony geometry and cell mechanics and facilitated us to characterize the correlation of cytoskeletal order with cell force generation for cardiac myocytes in detail.

Results

Membrane fabrication and application

Micropatterning of substrates resembling natural elasticities to eliminate artificial cell behavior and also to allow cell mechanical analyses on defined cell colonies was hardly possible with existing techniques. For this reason we adapted and further developed a technique based on work by Whitesides and coworkers[1,15,16] to create micro-colonies on even very soft silicone rubber substrates. The method is based on microstructured epoxy lift-off membranes whose fabrication is stated in detail in the Experimental section and in the schematic outline of Fig. 1. The initial step in membrane fabrication was the generation of a micro-structured photoresist layer of 25 μm in height on a silicon dioxide support. A heat-curable elastomer based on polydimethylsiloxane (Sylgard 184) was poured over the master and cured, providing a micro-structured stamp. After placing the stamp onto a glass slide, epoxy resin was disposed at the stamp boundary to fill up the thin gap between the stamp and the glass bottom by capillary suction. After curing of the epoxy resin, the stamp was

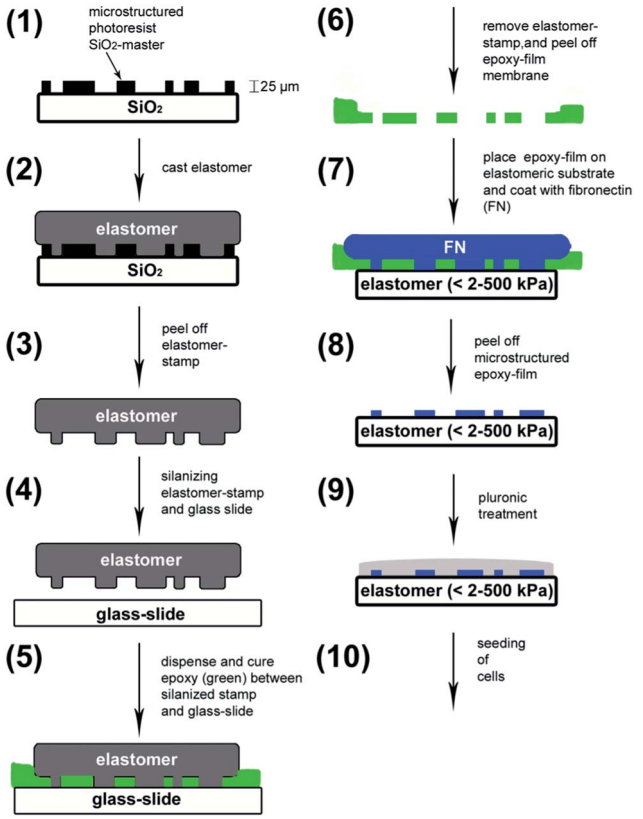

Fig. 1 Schematic outline of microstructured epoxy lift-off membrane fabrication. (1) The initial step for membrane fabrication is the production of a micro-structured SU-8 photoresist (25 µm thickness) on a silicon support. (2) An elastomer prepared from poly(dimethylsiloxane) (PDMS, Sylgard 184, base to curing agent 10 : 1) is poured over the master and cured at 60 °C for 2 h. (3) The PDMS-stamp is then peeled off the silicon master. (4) PDMS-stamp and a glass slide become silanized trichloro(1*H*,1*H*,2*H*,2*H*-perfluorooctyl)silane. This step reduces the adhesive forces between the PDMS-stamp as well as the glass slide and the cured epoxy membrane so that the epoxy film can easily be peeled off. (5) The silanized PDMS-stamp is placed on the silanized glass slide. The epoxy resin is then dispensed by capillary suction between the stamp and the glass slide. (6) After curing of the epoxy resin, the stamp is removed and the microstructured membrane is peeled off the glass slide. (7) In the next step the membrane is placed on soft elastomer substrates and coated with extracellular matrix proteins *e.g.* fibronectin (FN). (8) After discarding the FN solution, the membrane is removed gently from the soft substrate leaving the microstructured FN coating. (9) By blocking the non-FN coated area with a Pluronic F-127 solution to prevent cell adhesion, cells can be seeded (10) and adhered at predefined areas only.

removed from the glass slide and the cross-linked epoxy membrane could be peeled off. Resulting membranes comprising different microstructures (membrane A with small squares and rectangles and membrane B with lines of varying widths) are shown in Fig. 2A and B as scanning electron (SEM) micrographs. Micro-structured epoxy membranes were approximately 25 µm thick and features were well molded as holes spanning the entire epoxy membrane. Edges were evenly cast no matter which structure size or aspect ratio was analyzed (Fig. 2). Furthermore, epoxy-membranes themselves exhibited smooth surfaces on both sides.

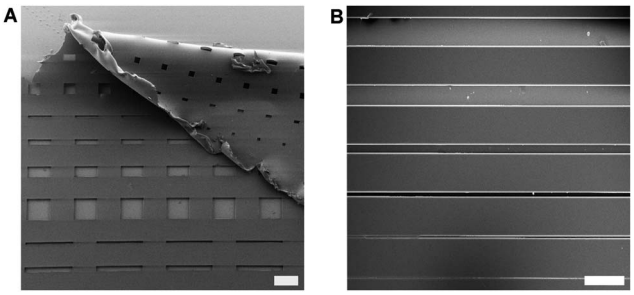

Fig. 2 Scanning electron micrographs of epoxy membranes. Two types of epoxy membranes consisting either of squares and rectangles of varying size (membrane A) (A) or lines of varying widths (membrane B) (B) were gold sputtered and imaged. Note that the 2.5 µm line could not be generated by photo-lithography and was therefore not available as a cavity for lift-off membrane coating. Scale bars, A: 200 µm and B: 100 µm.

Observation of epoxy–elastomer interplay and imbibition

Surface tension of the fluid and its contact angle to the capillary walls are major determinants of capillary suction and were therefore measured. For the contact angles of epoxy resin to silanized glass and the silanized silicone elastomer we obtained 74° and 82°, respectively (Table 1). The standard deviation of repeated measurements amounted to 3° and 5°. These values were obtained on small drops deposited on flat substrates. Moreover, the contact angle of epoxy resin to silanized silicone could be also observed from microscopic observation of imbibition (Fig. 3A). From such micrographs we obtained a contact angle of 73° with a standard deviation of repeated measurements of 2°. This value measured on a steadily advancing meniscus coincides within experimental uncertainty with the one measured on a sitting drop.

The interface tension between ambient air and epoxy resin was determined by the Wilhelmy plate method. We obtained a value of 70 mN m^{-1} with an uncertainty of 11 mN m^{-1} that is mostly due to the scatter of the contact angle measurement.

During steady advancement of the resin through the microstructure of membrane A we observed velocities of the meniscus ranging from 6 to 9 µm s^{-1} (Fig. 3A). Moreover, here the interface underwent marked edge pinning (Fig. 3B). During pinning the visible curvature of the meniscus changed from concave to convex with accordingly high changes in angles between the meniscus and silicone structures. Moreover, the

Table 1 Summary of measured contact angles of epoxy resin on different substrates

Epoxy resin to:	Contact angle [°]	s.d.	*n*
Glass	22	3	6
Glass silanized	74	3	6
Sylgard 10 : 1 silanized	82	5	6
Sylgard 10 : 1 silanized (imbibition)	73	2	40
Sylgard 15 kPa	69	10	6
Sylgard 1.5 kPa	88	7	6

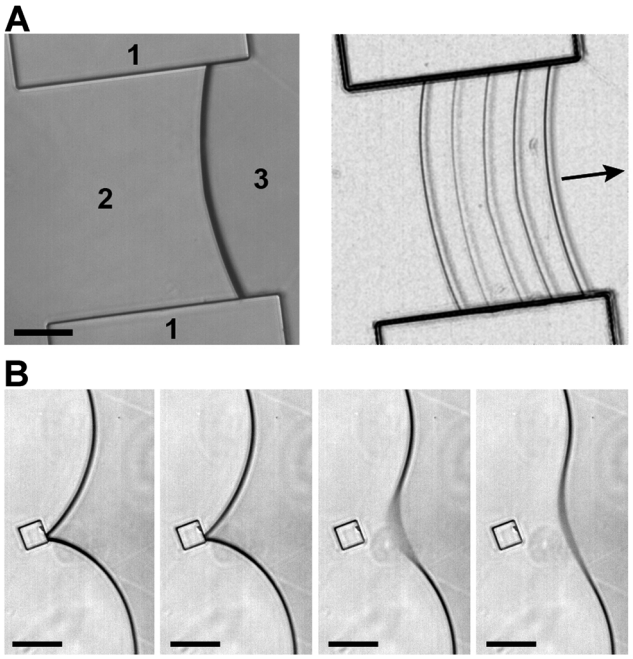

Fig. 3 Imbibition analyses: (A) advancement of epoxy resin through the silicone structure. Left: bright field micrograph showing the silicone structure (1), resin (2) and air (3). Scale bar, 50 μm. Right: overlay of thresholded micrographs (contrast enhanced) taken at intervals of 4 seconds. The arrow indicates the direction of motion. In this specific case the meniscus moved at 6.8 μm s^{-1} and exhibited a contact angle of 75° to silicone. (B) Pinning of the advancing meniscus at edges. Time series (interval 0.1 s) of bright field micrographs, direction of motion from left to right. Note the motional blurring in the right two micrographs. Scale bars, 50 μm.

meniscus was barely moving during pinned episodes. In contrast, very high velocities occurred during snap-off. In the case of Fig. 3B the maximum speed was estimated to about 400 μm s^{-1}.

The cured membranes displayed smooth surfaces and fairly rigid material behavior. The actual Young's modulus was determined by stepwise bending of a thin plate of cured epoxy resin. The material responded linearly and reversibly to the deformation. A slight viscoelastic relaxation was seen. With a 30 s relaxation period after each step and averaging over loading and unloading curves we found a Young's modulus of 2 GPa, comparable to familiar plastics listed in ref. 38 like polystyrene, 2.4–3.2 GPa, or polycarbonate, 2.1–2.4 GPa.

Since we wanted to use epoxy membranes to generate defined μ-colonies of mammalian cells on soft silicone rubber substrates, we tested the adhesiveness between epoxy membranes and silicone rubbers of varying elasticity. After attachment, epoxy membranes could be peeled from silicone rubber substrates of 10 kPa and stiffer without visible surface damage as analyzed by bright field microscopy.

Cell patterning on soft silicone rubber substrates

In order to generate defined μ-colonies of mammalian cells, membranes were placed on silicone rubber substrates of varying elasticities (1.5–100 kPa) to enable elastomer surface coating with extracellular matrix molecules (ECMs) through epoxy membrane microholes. Right after coating the membrane was removed and non-ECM coated surface areas of the elastomer substrates were blocked with Pluronic F-127. A primary isolated mixture of cardiac myocytes and cardiac fibroblast was added to the micropatterned substrates and cell adhesion was analyzed after 6 hours. No matter which substrate elasticity was analyzed, areas surrounding adhesive islands were always effectively blocked for cell adhesion (Fig. 4). Few isolated cells still visible were inefficiently adhered with mainly round cell shapes. Even after longer incubation periods of two days Pluronic-127 coats remained fully active with basically no cell adhesion around adhesive islands (data not shown). In contrast to surrounding surface areas, cell recognition of patterned structures was highly effective on all soft substrate elasticities down to 15 kPa (Fig. 4A and C, only shown for soft 15 kPa substrates). Small adhesive squares of 25 × 25 μm were formed and subsequently recognized by cells even in direct contact to large structures of 400 × 400 μm (Fig. 4A). Similar results of stable cell adhesion and cell shape adaptation were also

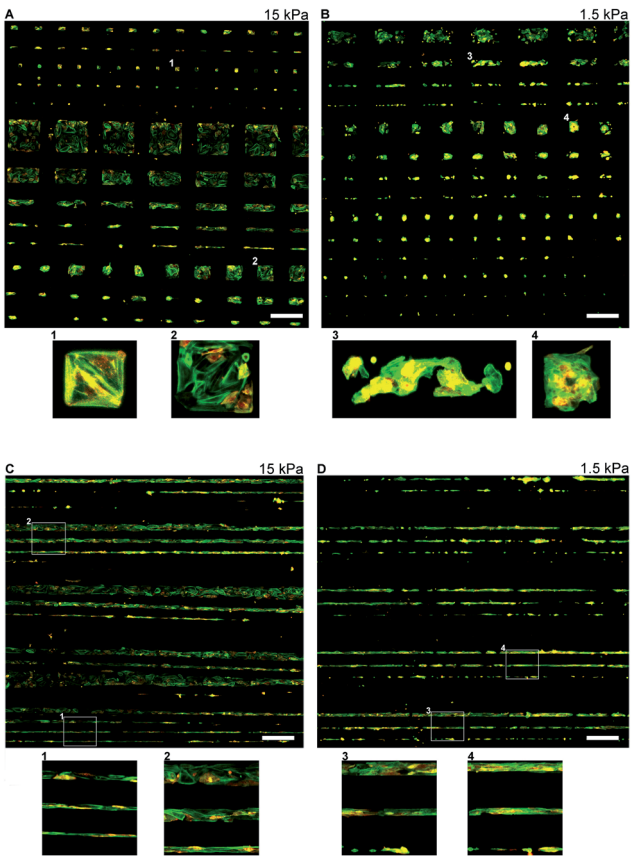

Fig. 4 Defined cell cluster formation. Squared and rectangular pattern shaped (A and B: membrane A) as well as line shaped (C and D: membrane B) 2-D cell clusters of primary myocardial cells were generated on soft (15 kPa) (A and C) and ultrasoft (1.5 kPa) (B and D) silicone rubber elastomers. Cells were stained for actin (green) and α-actinin (red). Magnifications below indicate cell clusters or regions indicated in the overview images. Scale bars, 400 μm.

observed for long lines of varying widths with a limit in line width recognition of 10 μm (Fig. 4C, membrane B).

For elastomeric substrates of even lower stiffness (1.5 kPa) generation of adhesive islands was still possible. While small squares and rectangles were visibly affected in reproducing shape accuracy of the epoxy membrane on soft substrates, larger structures and especially lines were sufficiently well formed and subsequently recognized by cells (Fig. 4B and D). However, line widths on 1.5 kPa were larger than expected when compared to the original lines used for patterning and very slight elastomer surface damage could be observed under the light microscope after lift-off membrane removal.

To determine whether the lower limit for cell recognition of features transferred through epoxy membranes in the range of 25 μm for squares and 10 μm for lines was due to incomplete pattern transfer or due to the limited cell adhesion area we used epoxy membranes (membrane B) and coated soft 1.5 kPa elastomeric substrates through the features with fluorescently labeled fibronectin. After membrane removal those substrates were used to analyze the efficiency of ECM surface coating and cell adhesion (Fig. 5A). The results prove ECM coating for all feature sizes used. Also lines with 10 μm and even 5 μm (Fig. 5C) in width were well visible with protein densities comparable to all other coated structure sizes. However, cell adhesion was already affected on line widths of 10 μm. Here as well as on 5 μm thin lines only a very low number of cells bound the coated areas exhibiting a rounded shape and no detectable cell cycle over time as analyzed also with 3T3 fibroblast cells (Fig. 5C).

The accuracy of adhesive pattern formation and subsequent cellular edge recognition was analyzed in more detail on various substrate elasticities. Protein transfer through epoxy membranes resulted typically in either very accurate borders (top border, Fig. 5B) or in borders with small semi-circular defects (lower border, Fig. 5B). Fluorescence micrographs indicated completely coated areas in between with 200 to 400% variations in protein density. The softer the elastomeric substrate was, the more often defects were observed. On elasticities above 15 kPa, defects were basically absent (data not shown). To verify possible reasons for defect formation on very soft silicone rubber substrates we analyzed the contact area of 50 kPa and 1.5 kPa silicone rubber with epoxy membranes at microholes (Fig. 5D). Confocal *Z*-stacks prove very clearly for 1.5 kPa substrates a bulged silicone rubber within cavities with local contact to epoxy cavity walls. Bulging and therefore wall contact could rarely be observed on stiffer 50 kPa substrates. Therefore we concluded that local wall contacts might be responsible for the slightly increasing surface area or coating defects observed on very soft substrates after membrane removal.

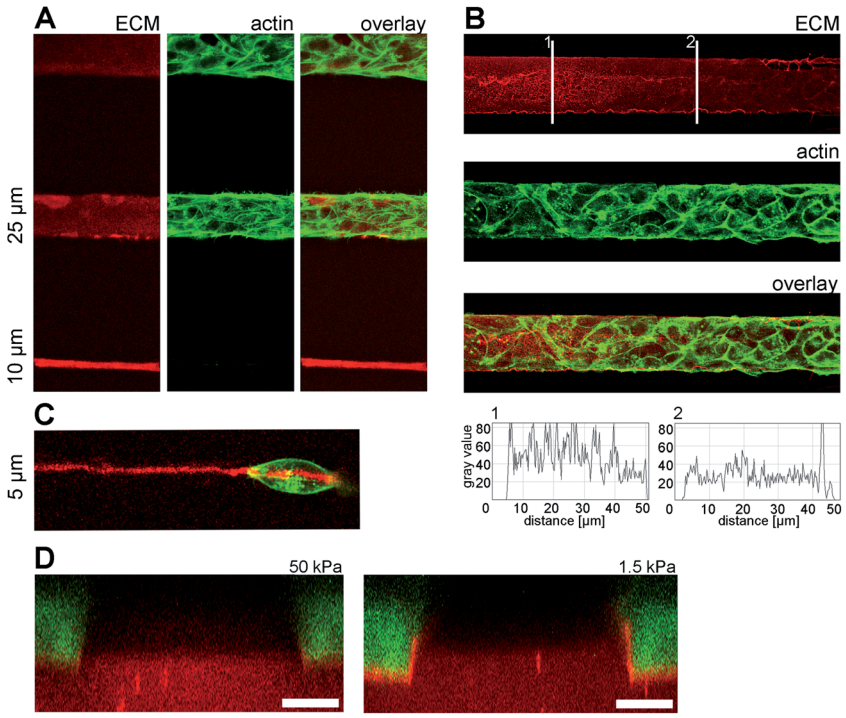

Fig. 5 (A) Using epoxy membranes thin lines of fluorescently labeled fibronectin (red) were generated on ultrasoft 1.5 kPa substrates and subsequently incubated with cells. After growth for two days, cells were fixed, stained for actin (green) and analyzed for cell adhesion depending on feature widths. (B) Lines of 25 μm in width were formed as in (A) and analyzed for homogeneous and stable fibronectin coating (red) after two days of cell adhesion (green, actin). Fluorescence intensities were determined along lines (1 and 2) and are given as gray values below. (C) A single 3T3 fibroblast adhered round-shaped to a 5 μm coated line. (D) Epoxy membranes were attached to soft (50 kPa) and ultrasoft (1.5 kPa) DiD pre-stained silicone rubber substrates. Subsequently, confocal *Z*-stacks were taken at cavity sides visualizing silicone rubber (red) and auto-fluorescence of epoxy membranes (green). For ultrasoft elastomers note the bulged silicone rubber within cavities with local contact to epoxy cavity walls while stiffer elastomers barely bend into cavity lumen.

Combination of defined cell shapes with traction force microscopy

The ability to dictate cell shape on soft silicone rubber substrates let us ask how overall myofibril organization as force generating units of cardiac myocytes influences total cell forces. Keeping the adhesion area constant various shapes were generated (Fig. 6A) on soft 15 kPa elastomeric substrates. No matter which predefined shape was analyzed, myofibrils were always formed as indicated by sarcomere formation and well visible *Z*-band staining. However, overall myofibril alignment was largely affected from largely unordered on round structures to well aligned on rectangular adhesion areas. Cells of triangular or squared shape were characterized by bundles of myofibrils aligned along area edges, therefore giving a mix of enhanced alignment on the small spatial scale and low alignment on the overall cell level.

Since cardiac myocytes are driven by stable contraction amplitudes causing continuously elevating force values with increasing substrate stiffness,[39] we analyzed whether the predefined cell shape and therefore overall myofibril organization within the cells would affect generated force values while keeping the substrate elasticity constant. Cells, shaped as given in Fig. 6A, were analyzed for overall contractile force values on 15 kPa substrates (Fig. 6B). Interestingly, no significant correlation between overall myofibril order and contractile forces could be identified with average force values in the 75 nN range (Fig. 6C). Furthermore, these values were comparable to those of cells that adhered to overall homogeneously coated substrates.[39]

Keeping the width of cells constant, rectangular shaped cardiac myocyte single cells were compared to cell clusters composed of two cells. While single cells were characterized by an adhesion area of 1040 μm^2 (s.d. 204 μm^2) on average, clusters of two cells adhered over an area of 1280 μm^2 (s.d. 148 μm^2). Upon cell–cell contact formation myocytes therefore reduced their adhesion area per cell, resulting in a still incomplete fill-out of the 1500 μm^2 adhesion areas in the longitudinal direction. Spontaneous beat frequencies of rectangular single cells and cell clusters were comparable with beat frequencies of about 1 Hz (s.d. 0.66 Hz). Overall contractile forces of two-cell clusters however clearly indicate an additive contractile cell behavior. With 119 nN (s.d. 74 nN) two-cell clusters were significantly stronger than single cells (Fig. 7A and B). As sites of cell–cell contacts no substrate deformations could be visualized (Fig. 7A) arguing for stable cell–cell contact formation and contraction as functional unit as known for natural myocard tissue.

Discussion

Generation of defined single cell or cell cluster shapes on soft elastomeric substrates is of urgent need for biotechnological and medical applications. Hereby mechanical signals *i.e.* in this case elasticity and topography can be ideally combined with chemical factors in order to direct cellular function in directions of natural *in vivo* behavior. Separately, elasticity as well as cell shape or size definition are well known to regulate cellular processes from simple functional adaptations to complex differentiation processes.[5,25,40–42]

However, combining both mechanical parameters remained challenging due to severe technical problems with reproducible

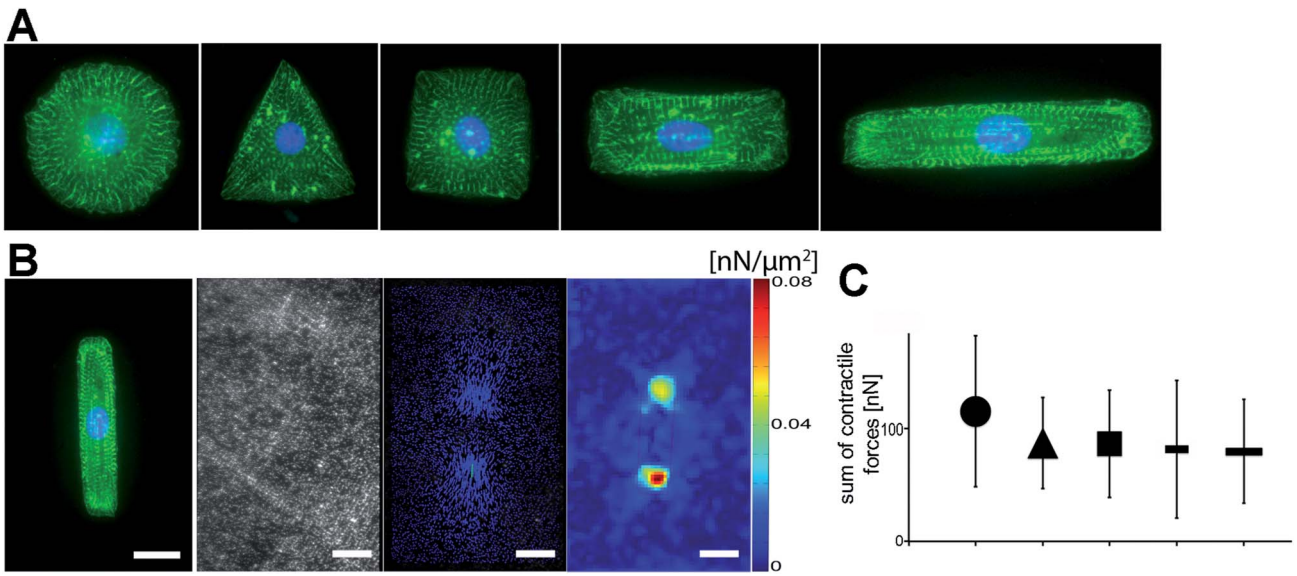

Fig. 6 (A) Defined adhesion patterns of approximately 1500 μm^2 and round, triangular, square or rectangular shape were formed using epoxy membranes on silicone rubber substrates (15 kPa) labeled with fluorescent beads (not shown) (for exact dimensions see Experimental). Cells were fixed and stained for α-actinin (green) and nuclei (DAPI, blue). (B) Traction force microscopy of shaped cardiac myocytes were performed over at least 4 spontaneous contractions each. Substrate deformations were visualized by following displacements (second right) of substrate incorporated beads (second left) and subsequently back-calculated into forces (right). Following experiment, cells were fixed and stained for α-actinin and nuclei (left). Scale bar = 20 μm. (C) Average sum of contractile forces including s.d. for cardiac myocytes with shapes as indicated. Number of analyzed cells: circle = 5, triangle = 14, square = 12, short rectangle = 5, long rectangle = 28.

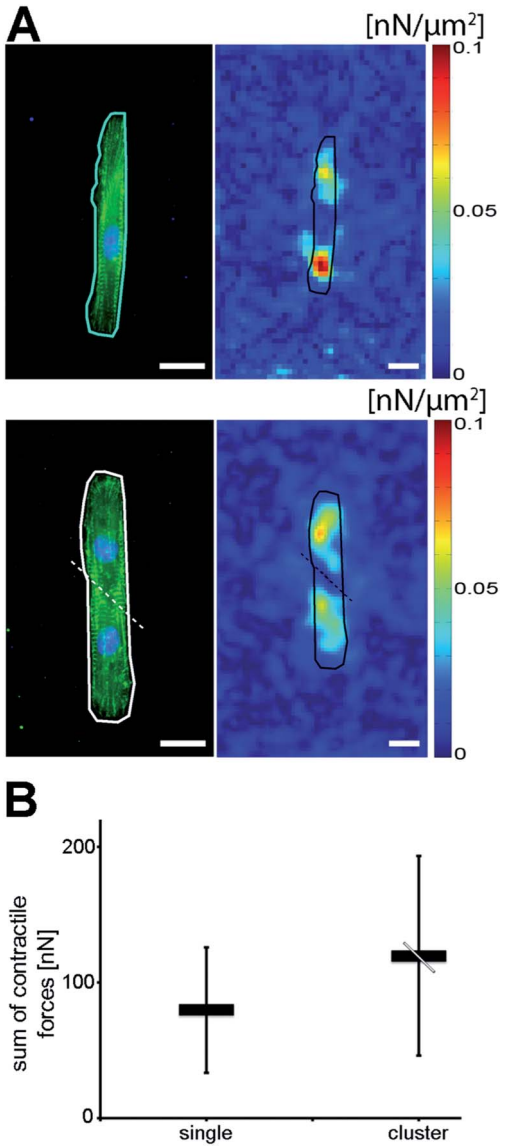

Fig. 7 (A) Traction force measurements (right) were performed on rectangular shaped cell clusters composed of two cells (bottom) and compared to those of single cells (top) of identical shape. After cell force calculation cells were fixed and stained for α-actinin (green) and nuclei (blue) (left). Cell–cell contact zone is indicated by a dotted line with no detectable force application beneath. (B) Averaged sum of contractile forces for single rectangular shaped cells (single, $n = 28$) and cell clusters (cluster, $n = 6$). Note that none of the analyzed cells/cell clusters was impaired by the limited adhesion area in the longitudinal direction.

and fast elastomer functionalization at distinct spots with defined molecules. When using polyacrylamide hydrogels surface functionalization with proteins to induce cell adhesion depends on complex protocols covalently coupling either reactive amines on proteins *via* sulfo-SANPAH or carbohydrate groups on proteins *via* hydrazine hydrate to PAA gels.[33,43] Latest developments have simplified chemical functionalization to EDC–NHS coupling after deep UV-illumination[44] or use of activated proteins.[45] Comparable coupling reactions are used for PEG-based hydrogels. While those elastomers are often used for direct three-dimensional pattern formation,[31,46] surface functionalization with proteins depends as well on covalent coupling using chemicals as *e.g.* 5-azidonitrobenzoyloxy-NHS.[47] Those coupling procedures can hamper formation of defined adhesion areas on flat hydrogel surfaces or might lead to surface stiffening.[44]

Instead, defined islands for cell adhesion are often generated either by micro-contact printing (μCP) using stamps or by lift-off membranes for structuring stiff surfaces. While stamps are most often made of silicone rubber able to transfer molecules to feature sizes down to around 50 nm edge length,[48,49] lift-off membranes can be generated by various means as *e.g.* electron-beam lithography on PMMA films,[50] pattern transfer from silicon masks to vapor deposited parylene C films,[32,51] spin-coating of uncrosslinked silicone oils over silicon masks and subsequent cross-linking[13,14] or use of epoxy resins filling free spaces of silicone rubber stamps.[52] However, using μCP or lift-off membranes for structuring soft elastomers with cell adhesion inducing molecules is extremely challenging. Examples for patterning parylene C films by covalent protein coupling[32] or polyacrylamide gels are described.[53,54] However, major technical problems of either insufficient sealing after contact between micro-structured membrane and elastomeric substrates (most lift-off membranes on hydrogels) or too effective stickiness and therefore substrate rupture upon stamp/membrane removal (*e.g.* silicone rubber lift-off membranes on soft silicone rubber substrates, here most likely mainly due to identical material properties) hamper the use of techniques ideal for defined cell shape generation on soft substrates. The central goal of our methodology was therefore finding and characterizing a material useful for efficient and accurate lift-off membrane formation with subsequent adhesive membrane properties high enough for good sealing but low enough for rupture-free separation after elastomeric surface structuring.

Lift-off membrane formation of our methodology essentially depends on filling of the channels and free spaces formed between the silanized silicone rubber structure and the also silanized glass substrate without formation of air bubbles or other defects. Filling this microstructure with epoxy resin is affected by capillary action and, in essence, a process of microfluidics.[55,56] For the description of our observations Reynolds number, $\mathrm{Re} = \rho u h/\mu$, and capillary number, $\mathrm{Ca} = \mu u/\sigma$, are the most important characteristics describing the flow and the meniscus shape. Here, ρ denotes the fluid density, μ the viscosity, σ the surface tension, u the velocity and h the channel height. Extremely small Reynolds numbers of 5×10^{-7} in steady advancing flow and 4×10^{-5} during release of pinned interfaces indicate the irrelevance of inertia forces and strictly laminar flow. For these estimates we used our measured values of surface tension, meniscus speed, and structure height as well as the manufacturer's values for density (1.14×10^{3} kg m^{-3}) and viscosity (0.45 Pa s) of the epoxy resin (Technical data sheet Epo-Tek UVO-114, Rev. IV 08/2007, Epoxy Technology Inc, Billerica, MA). In steady advancing flow capillary numbers are very small, 5×10^{-5}, thus surface tension dominates by far over viscous forces. Therefore shapes of moving interfaces can be well approximated by those known for stationary ones. However,

during sudden release of fluid surfaces pinned at edges (*cf.* Fig. 3B) much higher velocities occur resulting in capillary numbers of about 5×10^{-3}. In line with these values we observed almost perfectly circular meniscus shapes during steady advance (radius of curvature $\approx$ 300 μm in Fig. 3A) and significant deviations from circularity during pinning and release of pinning (*cf.* Fig. 3B).

As surface tension dominates over viscous forces capillary suction pressure can easily be calculated from the Young–Laplace equation (eqn (3)) combined with geometrical or energetic considerations. In essence, the meniscus curves in two main axes oriented along the geometry of the rectangular cross-section of the gap. Denoting the contact angle of epoxy resin to silanized glass with Θ_g and the one to silanized silicone with Θ_s, channel height with h and width (at the location of the meniscus) with w the equations given by ref. 20 can be expressed as

$$\Delta p = p_w + p_h = \sigma \frac{2 \cos \Theta_s}{w} + \sigma \frac{\cos \Theta_s + \cos \Theta_g}{h} \quad (1)$$

In our system the contribution due to the channel height, p_h, amounts to 1.5 kPa. The second contribution due to the channel width varies locally within membrane A and, for the case of Fig. 3 amounts to 0.16 kPa.

Very important for filling of interconnected channels *e.g.* in our membrane A is that the overall fluid front stays relatively flat, *i.e.* that the fluid in one channel is not much faster than in others. Based on an approximate expression for channel flow resistance cited by Tabeling[56] we estimate the pressure drop over a channel as shown in Fig. 3A (200 μm width and 200 μm length) to only 10% of the overall capillary suction. In other words, for reasonable geometry interconnections between different straight channels are frequent enough to relieve different pressure drops due to different channel widths by transversal flows before air entrapment due to filling a channel simultaneously from both sides can occur.

Related considerations have been presented for flow in Hele-Shaw cells exhibiting random patterns of flow resistance.[57–59] This pattern results in a roughening of the moving fluid front whereas two effects tend to straighten it. The first effect is that the further a piece of contact line advances the higher the flow resistance gets. This acts at long length scales and parallels the argument given here. The second factor straightening the interface at small distances is interface tension. The action of this effect is dramatically demonstrated during breakage of interface pinning (*cf.* Fig. 3B). Indeed, the speed of the meniscus seen in Fig. 3B corresponds reasonably well to time scales estimated for surface tension driven relaxation from equations given in ref. 59.

Pinning of the fluid–air interface at edges opposes filling (*cf.* Fig. 4). This process has been carefully characterized by Berthier and coworkers for interfaces between different fluids.[60] Their results can easily be transferred to the case of air–fluid interfaces. They find that rectangular obstacles exhibit the highest potential for pinning. During pinning the curvature of the meniscus in height direction remains almost unchanged, however, in the width direction it even changes its sign. For two pillars or rectangles at a distance w, Berthier *et al.* show that the maximum counter-pressure corresponds to a fluid front forming a right angle with the pinning surface, *i.e.*, the radius of curvature along the width is then $-w/2$. In the case of Fig. 3B the distance is 200 μm and, indeed, circles with radii of 100 μm fit very well to the meniscus close to the contact point. Thus at pinning sites the total suction pressure amounts to

$$\Delta p = p_w + p_h = -\sigma \frac{2}{w} + \sigma \frac{\cos \Theta_s + \cos \Theta_g}{h}. \quad (2)$$

As contact angles are rather close to 90°, the counter pressure by pinning is severe. For Fig. 3B it is −0.7 kPa, *i.e.*, it reduces the total suction to about 50%. Structure filling will stop being reliable as soon Δp becomes zero at pinning sites. That is, as soon as $w < 2h/(\cos \Theta_s + \cos \Theta_g)$. In our case, corners at intersections have to be at least 93 μm apart. Smaller values require either very rounded shapes (see ref. 60), lower channel heights or lower contact angles.

Reducing channel heights would increase flow resistance and filling times whereas slightly lower contact angles are feasible by careful tuning of the surface properties. However, this strategy has already been systematically explored by Kim and Whitesides.[19] These authors find at high energy interfaces, corresponding to low contact angles, precursor flows and edge flows that pose a high risk of air entrapment. Moreover, along a more practical argument, high energy surfaces between resin and the substrate are in almost all cases also causing high energies of adhesion between cured resin and the rigid substrate. While the high stiffness mismatch between cured epoxy (2 GPa) and our silicone rubbers (in the 10 to 100 kPa regime) somewhat facilitates the peeling process by focusing vertical stresses in small regions, very soft silicone rubbers are extremely tacky and easily deformed. This is witnessed by the semi-circular edge defects found on the softest silicone cell substrates used (*cf.* Fig. 5). Therefore the very high contact angles of more than 70° observed here are a necessity for our experiment and even allows generation of very small structures in direct proximity to much larger ones as long as the distance w is above the 93 μm given above. Their detrimental effect on capillary suction is partially offset by the very high surface tension of the epoxy resin. Therefore capillary filling still occurs rapidly enough to be of practical use.

Attractive forces based on mainly surface tension and hydrophobic interactions between epoxy lift-off membranes and soft silicone rubber substrates highly efficiently seal contact areas in our experiments. This can be seen by an almost perfect replica formation of adhesive islands through micro-cavities of epoxy membranes with shape sizes down to 2.5 μm (*cf.* Fig. 5). Accurate surface patterning works well down to substrate elasticities of approximately 10 kPa. Only on very soft silicone rubber substrates (1.5 kPa) surface tension and substrate elasticity lead to elastomer creeping on cavity walls generating artifacts upon membrane removal especially for small cavity areas.

When cell adhesion and growth was analyzed along our thin adhesive lines of widths down to 10, 5 and 2.5 μm on soft substrates we could identify impaired adhesion and growth on

10 μm lines and even fully blocked adhesion on 5 and 2.5 μm thin lines. These data are in very good agreement with former results obtained on stiff substrates. Here, cells grown on printed lines of 10 μm width stopped growth and underwent apoptosis over time.[5] Even neuronal cells, characterized by very thin extensions, highly depend on line widths at least at nuclear sites of around 20 μm for proper growth and differentiation.[6] Those results on artificial stiff substrates are therefore in very good agreement with our findings of limited (10 μm) or even fully blocked cell growth (5 and 2.5 μm) thin adhesion lines on soft substrates mimicking natural elasticities.

Furthermore, using our technique homogeneity of coating by physisorption through micro-cavities was similar to complete surface coating without the use of lift-off membranes. Small variations in concentration of physisorbed proteins could be identified (*cf.* Fig. 5B) but at no time any correlation of cell morphology or function with those variations could be seen. Even cell culturing over several days did not lead to cell detachment or outgrowth from predefined adhesion areas arguing once again for homogeneous protein coating within adhesion areas and efficient blocking only around them by a dense brush-like Pluronic conformation on top of silicone rubber.[61]

Using our lift-off membranes we were able to direct the cell shape of late embryonic cardiac myocytes thereby regulating overall myofibril order. While myofibrils were shown to be equally present on any elasticity from 1 kPa to 500 kPa, cell forces elevated with increasing substrate stiffness due to an amplitude driven contractile behavior.[41] However, it was unclear whether myofibril alignment might elevate force generation. We therefore forced myocytes into shapes on 15 kPa substrates known to represent natural tissue elasticity.[62,63] As a result identical myofibril overall alignment could be identified as described before[64] ranging from very low alignment (circle) to high myofibril order (rectangles). Interestingly, different organization levels had no significant effect on force generation with highly comparable sum of contractile forces for all analyzed cell shapes. These data indicate that the aspect ratio and overall cytoskeletal organization are just minor regulatory factors for force generation in cardiac myocytes.

Furthermore, single cell force values of rectangular cells were compared to those of two-cell clusters on rectangles of identical width. The reduced covered substrate area per cell in two-cell clusters indicates stable formation of cell–cell contacts. On the level of traction forces no substrate deformations were identified at sites of cell–cell contacts. These data are in very good agreement with those of McCain and coworkers[65] showing that functional cell–cell contacts between myocytes are formed in a time dependent manner. While shortly after adhesion focal adhesions are still present at cell–cell contact sites, those matrix adhesions disappear to form functional cell-spanning units over time. In our system this led to coordinated contraction behavior and clearly elevated force values for the two-cell cluster, therefore mimicking cardiac myocyte behavior in myocard tissue. Comparable studies measured forces at cell–cell junctions of 20 to 200 nN for non-muscle cells[66,67] and up to 1000 nN for cardiac tissue.[65] This argues once again for tight intercellular interactions between cardiac myocytes and proves the importance to analyze the cardiac cell function *in vitro* on soft substrates with single cells and cell clusters of defined, nature mimicking shape.

Experimental

Preparation of elastomeric silicone rubber substrates

Elastomeric substrates were made of Sylgard 184 Silicone Elastomer Kit (Dow Corning GmbH, Wiesbaden, Germany) as previously described.[68] In brief, both components (base and cross-linker) of the elastomer kit were mixed at various ratios to generate after cross-linking either stamps from silicon wafers (10 : 1 (w/w)) or cell culture substrates (70 : 1 (1.5 kPa), 50 : 1 (15 kPa), 40 : 1 (50 kPa), and 35 : 1 (100 kPa)). For some experiments 50 : 1 silicone substrates were microstructured with red fluorescent beads (0.2 μm diameter, FluoSpheres crimson carboxylate-modified beads, Invitrogen, Darmstadt, Germany) as described.[69] The elastomer layer thickness was adjusted to 80 μm using glass slices of defined thickness (Menzel GmbH, Braunschweig, Germany) as spacers. Cross-linking of silicone oils was performed at 60 °C for 16 h. After curing, elastomeric substrates were glued to the bottom of 3.5 cm Petri-dishes to cover predrilled holes. Mechanical properties of all elastomeric mixing ratios were characterized as described[68] resulting in elasticities as given above and a Poisson's ratio of 0.5. If necessary, silicone rubber substrates were stained with the hydrophobic dye DiD Vybrant cell-labeling solution (Molecular Probes, Eugene, OR) in a 1 : 300 dilution. Staining was performed at 37 °C for two days.

Lithographic techniques

Silicon wafers were preheated at 180 °C for 30 min and overlaid with a 25 μm thick layer of SU-8-25 photoresist (Microchem, Newton, MA). Subsequently the photoresist layers were soft-baked for 2 min at 65 °C followed by slow ramp heating to 90 °C within 5 min and additional baking of the photoresist at 90 °C for 2 min. Using ultraviolet-photolithography at 346 nm with a source power of 7 mW for 25 s, the structures of photolithography masks were transferred into the photoresist layer. The lithography masks themselves were written using an electron beam lithograph and consisted either of lines with widths of 2.5, 5, 10, 25, 50 and 75 μm, respectively (membrane B) or rectangles and squares of varying sizes (membrane A: square sizes of 400 × 400, 200 × 200, 100 × 100, 50 × 50 and 25 × 25 μm and starting from those squares, rectangles with a repetitively bisected width down to 25 μm). For traction force microscopy experiments membrane C was generated exhibiting various geometries with rectangles (17 × 86 and 15 × 104 × 75 μm), squares (lateral length = 39 μm), equilateral triangles (lateral length = 60 μm) and circles (diameter of 22 μm) resulting in an adhesive area of approximately 1500 μm^2 for all geometries. Cell clusters composed of two cells were exclusively analyzed on 15 × 104 μm rectangles. Each wafer was post-baked for 1 min at 65 °C followed by slow ramp heating to 90 °C within 5 min and additional baking for 1 min at 90 °C. The

uncross-linked photoresist was removed using an SU-8 developer (Microchem, Newton, MA, USA) for 6 min. Finally, the photoresist was hard-baked for 30 min at 180 °C. The SU-8-25 wafers were then silanized by exposure to vapor of trichloro(1*H*,1*H*,2*H*,2*H*-perfluorooctyl)silane (Sigma-Aldrich, St. Louis, MO, USA) in a vacuum for 30 min at room temperature.

Epoxy membrane preparation

For silicone rubber stamp formation, small cylinders (1.5 cm height, 0.5 cm diameter) were placed onto microstructured wafers, filled with uncrosslinked elastomers (10 : 1 ratio, Sylgard, Dow Corning, USA) and the contents were cured at 60 °C for 30 min (see Fig. 1). For epoxy membrane fabrication stamps as well as glass slides were silanized (trichloro(1*H*,1*H*,2*H*,2*H*-perfluorooctyl)silane, Sigma-Aldrich) at room temperature for 30 min in a vacuum. This silanization step minimizes the existing adhesive forces between the epoxy and the PDMS-stamp as well as the adhesive forces between the epoxy and the glass slide, which ensures the easy removal from the glass support after curing. After silanization stamps were placed onto silanized glass slides with an additional weight of approximately 30 g on top. For the preparation of the membrane we used an optically transparent, UV-curable epoxy resin (EPO-TEK UVO-114, Epoxy Technology, Billerica, MA, USA). Uncured epoxy resin was placed at the stamp boundary from where it filled the gap between the stamp and the glass slide due to capillary forces. Hardening of the epoxy resin was performed by UV exposure on a transilluminator table (ELX-FI5M; Vilber Lourmant, Marne Le Vallee, France) for 40 min. After curing, the stamp was removed and the membrane was peeled off the glass slide.

Epoxy membrane elasticity measurement

The Young's modulus, E, of cured epoxy was determined by beam bending. To this end we manufactured an epoxy plate (length, l, 52 mm, width, w, 11.3 mm, and thickness, h, 0.95 mm). The plate was centered over a gap of 36 mm in width. Force was applied exactly at the center of the gap by a hemispherical punch (4 mm diameter) attached to a force sensor (KD78 0.5 N; ME-Meβsysteme; Henningdorf, Germany) and moved by a linear translation stage (PICO Linear Axis LTP 60; Steinmeyer-FMD, Dresden, Germany). Loading was performed in 10 successive steps of 40 μm, each followed by a relaxation period of 30 s. Punch retraction was done identically. Forces were sampled at 10 Hz. For each step the indentation resistance, k, was calculated as the ratio of the equilibrium force (mean over the last 3 s) to the indentation depth (step height corrected for the stiffness of the force sensor). The material showed a linear and reversible response to the individual steps. For this geometry the Young's modulus was calculated according to $E = kl^3(4w)^{-1}h^{-3}$.

Preparation of microstructures from extracellular matrix protein on silicone rubber

Microstructured epoxy lift-off membranes were positioned on dry soft silicone rubber substrates and remained in place due to substrate stickiness (Fig. 1). Elastomer coating was performed through the microstructured holes of the epoxy membrane with human plasma fibronectin (5 μg ml^{-1}; BD Bioscience, San Jose, CA) diluted in phosphate buffered saline (PBS; 137 mM NaCl, 8 mM Na_2HPO_4, 2.7 mM KCl; 1.5 mM KH_2PO_4, pH 7.4) for 60 min at 37 °C. Placing of coating solution on top of the microstructured epoxy lift-off membrane can result in the formation of air bubbles trapped in some corners of the squares and rectangles or along the lines. Therefore we shortly and gently degassed the coating solution on top of the "lift-off" membrane, releasing the trapped air bubbles to ensure a precise fibronectin-coating within the microstructured boundaries. After discarding the coating solution the sandwich was washed twice with PBS. Then the membrane was removed from the substrate. This step was followed by treatment with 1% Pluronic F-127 in PBS (nontoxic triblock polymers (polyethylene glycol–polypropylene glycol–polyethylene glycol), Sigma-Aldrich) for 20 min at 37 °C to overlay uncoated surface areas and to block cell adhesion at those areas. Finally unbound Pluronic F-127 molecules were removed by repetitive (four times) washing steps with deionized water.

Cell culture

Cardiac myocytes were isolated from 19 day old Wistar fetal pups as described before (Hersch *et al.*, 2013). Isolated cells (65 000–80 000) were seeded over adhesive islands of silicone rubber substrates. Cells were maintained at 37 °C and 5% CO_2 in a humidified incubator and cultured in an F10 Ham's medium supplemented with 10% fetal bovine serum, a 1 : 100 dilution of an antibiotic solution (10 000 units penicillin and 10 mg ml^{-1} streptomycin in a 0.9% NaCl, Sigma-Aldrich) and a 1 : 200 dilution of solution containing insulin (1 mg ml^{-1}), transferrin (0.55 mg ml^{-1}), and sodium selenite (0.5 mg ml^{-1}) in EBSS (Earle's Balanced Salt Solution, Sigma-Aldrich).

Immunocytochemistry

Cells on microstructured silicone rubber substrates were fixed for 30 min in 3.7% paraformaldehyde (Merck, Darmstadt, Germany) in cytoskeleton-buffer (CB: 150 mM NaCl, 5 mM $MgCl_2$, 5 mM EGTA, 5 mM glucose and 10 mM 2-(*N*-morpholino)ethanesulfonic acid at pH 6.1) and permeabilized for 5 min at 37 °C with 1% Triton-X-100 in CB. After washing twice with CB, cells were treated with blocking-solution (5% skim milk powder in CB) for 45 min at 37 °C. Afterwards cells were incubated with a 1 : 100 solution of primary monoclonal mouse antibody against α-actinin, clone EA 53 (Sigma-Aldrich, St. Louis, USA) for 1 h at 37 °C. Cells were washed three times with blocking solution and then incubated for an additional hour at 37 °C with a 1 : 200 solution of a secondary Cy3-labeled antibody (Jackson Immuno Research Europe Ltd., Suffolk, UK). For visualizing the actin cytoskeleton Alexa 488-phalloidin (Invitrogen, Darmstadt, Germany) was added in parallel to the secondary antibody in a 1 : 100 dilution. Cells were washed with CB and purified water. For microscopic analysis, cells were embedded in 20 μl Fluoromount/DABCO solution (Sigma-Aldrich). Stained cells were analyzed with an inverted confocal laser scanning microscope (LSM 710, Carl Zeiss, Jena, Germany)

using a Plan-Apochromat 63× NA 1.4 oil immersion objective, a Plan-Neofluar 40× NA 1.3 oil immersion objective or a 10× EC Plan-Neofluar NA 0.3 PH1 lens (all Zeiss). For acquiring *Z*-stacks the Plan-Apochromat objective was used.

Traction force microscopy

For traction force microscopy on spontaneously contracting cardiac myocyte patches differently predefined cell shapes (membrane C) were generated on fluorescent bead microstructured soft (15 kPa) silicone rubber substrates. Cells were analyzed at 37 °C and 5% CO_2 using an inverted microscope (Axiovert Observer Z.1; Zeiss) equipped with a 40× EC Plan-Neofluar NA 1.3 oil immersion objective (Zeiss). Sequences of beating cells were captured with 50 frames per second and 2-fold digital binning using a sCMOS camera (Neo; Andor technologies, Belfast, Ireland). At least four spontaneous contractions per cell were captured. Measurement of bead displacements and subsequent cell force calculations were performed as described earlier.[70] For rectangular myocyte two-cell clusters (membrane C) substrate deformations at sites of cell–cell contacts were determined. Since no substrate deformation could be detected at those sites, myocyte clusters were assumed to act as units and analyzed for their overall force generation only. After traction force measurements all cells were fixed and stained with α-actinin and DAPI.

Contact angle measurements

Contact angles were measured with an optical contact angle measuring system (OCA 20; Data Physics Instruments GmbH, Filderstadt, Germany). Contact angles were determined by fitting to the both edges of small drops sitting on the respective substrates and are given as the mean of at least three repeated measurements on independent samples.

Surface tension measurements

The surface tension, σ, of the epoxy resin was determined by the Wilhelmy plate method. To that end a Petri dish filled with fluid resin was placed on a balance (Labstyle 204; Mettler-Toledo, Gießen, Germany) and a silanized coverslip was gently brought into contact with the fluid by a motorized linear translation stage (MDrive 23, Steinmeyer, Feinmeß Dresden, Germany). Forces were read out *via* the scale's serial interface at a rate of 6 Hz. Upon meniscus formation a sudden jump of force, F, was observed which amounts to $F = l\sigma \cos \Theta$, where l denotes the circumference of the coverslip and Θ the contact angle of epoxy resin on silanized glass as measured above. Four to five repeated measurements were performed on three separate coverslips. For validation of the setup the surface tension of water was measured using a clean glass plate (contact angle 0°). The result of 72 mN m^{-1} was in full accord with published values.[71]

Scanning electron microscopy

Scanning electron microscopy was performed using a Leo 1550 scanning electron microscope (Carl Zeiss, Jena, Germany). Before analysis, the microstructured membrane was coated with a 2–4 nm Pt/Pd layer using a sputter coater (Cressington 208 HR/MTM20, Watford, UK). Scanning electron microscopy was carried out at 10 kV using the InLens detector and a working distance of 3 mm. Composite electron micrographs of the epoxy membrane were assembled using Photoshop CS4 (Adobe, San Jose, CA, USA).

Observation of imbibition

In some cases the advancement of the epoxy fluid within the microstamp–glass sandwich was recorded. To this end the sandwich was placed on an inverted microscope (Axiovert 200 equipped with a 10× EC Plan-Neofluar NA 0.3 PH1 lens; both Zeiss) and images were taken at 10 Hz using a sCMOS camera (Neo; Andor, Belfast, UK). For better visualization of the advancing meniscus the find edges tool of Fiji[72] was used, the look-up table was inverted and snapshots taken at suitable time intervals were overlaid. In some cases the images were segmented before overlaying to improve visibility. To this end the threshold algorithm of Otsu[73] was used as implemented in Fiji. Contact angles of the moving meniscus to silicone rubber features and distances were measured by hand. The meniscus curvature was estimated by overlaying visibly fitting circles in Photoshop CS4.

Theoretical considerations

Microstencil formation, as performed here, crucially depends on filling a mold with epoxy resin without trapping air bubbles or generating other defects. The underlying basic process, imbibition of a fluid into the capillary, is driven by the surface tension, σ, of the fluid and the free energy of interaction between wall materials and fluid.[17–21] A convenient measure of these interactions is the macroscopic contact angle, Θ. On flat substrates, this parameter defines if a substrate is wetted by fluid.[74] At a vanishing contact angle a drop of fluid placed on a flat substrate spreads to form a, theoretically, infinitely thin film. At all other contact angles a finite sized contact area between fluid and the substrate is formed. At the three phase contact line where the free surface of the drop meets the substrate the macroscopic shape of the fluid surface forms the contact angle. At molecular length scales a precursor film of fluid often spreads beyond the drop covered area.[74]

Suction of a fluid into a capillary occurs if the contact angle between fluid and the wall material is below 90°. Here, a meniscus forms whose curvature is set by capillary geometry and contact angle. The suction pressure of the capillary is given by the law of Young and Laplace

$$\Delta P = \sigma(R_1^{-1} + R_2^{-1}) \quad (3)$$

It connects the pressure difference, ΔP, acting over a fluid interface with its interface tension, σ, and its curvature (principal radii of curvature R_1 and R_2). In rectangular channels a stable meniscus forms at contact angles above 45° as given in ref. 75. At lower values corner flow occurs where threads of fluid filling the sharp corners of the channel cross-section transport fluid far

ahead of the proper meniscus.[75–77] This fluid may indeed fill corners in the microstructure and thus entrap air. Another feature of the fluid front occurring at even lower contact angles is a precursor film that may even split (observed *e.g.* in ref. 19). Again this precursor is apt to transport fluid ahead of the meniscus to tight spots in the microstructure where it might seal exit paths for air. Taken together we arrive at the counterintuitive conclusion that bubble free filling of microstructures requires larger contact angles above 45°, *i.e.*, only weak attraction between fluid and the wall material. Moreover, observations of bubbles entrapped in microfluidic devices have shown that these tend to split at higher flow speeds.[76,78]

Acknowledgements

We thank Marko Banzet and the team of the Helmholtz Nanoelectronic Facility for intense technical support. Prof. Offenhäusser generously gave access to equipment. We also thank David Kirchenbüchler and Kevin Küpper for helpful discussions. This work was supported by the German Bundesministerium für Bildung und Forschung (BMBF, project title: MechanoSys, BMBF-Nr. 0315501A).

References

1 A. Kumar and G. M. Whitesides, *Appl. Phys. Lett.*, 1993, **63**, 2002.
2 D. Lehnert, B. Wehrle-Haller, C. David, U. Weiland, C. Ballestrem, B. A. Imhof and M. Bastmeyer, *J. Cell Sci.*, 2004, **117**, 41–52.
3 C. S. Chen, M. Milan, H. Sui, G. Whitesides and D. E. Ingber, *Science*, 1997, **276**, 1425–1428.
4 K. K. Parker, A. L. Brock, C. Brangwynne, R. J. Mannix, N. Wang, E. Ostuni, N. Geisse, J. C. Adams, G. M. Whitesides and D. E. Ingber, *FASEB J.*, 2002, **16**, 1195–1204.
5 L. E. Dike, C. Chen, M. Mrksich, J. Tien, G. M. Whitesides and D. E. Ingber, *In Vitro Cell. Dev. Biol.: Anim.*, 1999, **35**, 441–448.
6 L. Lauer, C. Klein and A. Offenhäusser, *Biomaterials*, 2001, **22**, 1925–1932.
7 S. A. Ruiz and C. Chen, *Stem Cells*, 2008, **26**, 2921–2927.
8 R. Fricke, P. D. Zentis, L. T. Rajappa, B. Hofmann, M. Banzet, A. Offenhäusser and S. H. Meffert, *Biomaterials*, 2011, **32**, 2070–2076.
9 M. Bray, S. P. Sheehy and K. K. Parker, *Cell Motil. Cytoskeleton*, 2008, **65**, 641–651.
10 M. L. Decker, D. G. Simpson, M. Behnke, M. G. Cook and R. S. Decker, *Anat. Rec.*, 1990, **227**, 285–299.
11 J. W. Sanger, S. Kang, C. C. Siebrands, N. Freeman, A. Du, J. Wang, A. L. Stout and J. M. Sanger, *J. Muscle Res. Cell Motil.*, 2005, **26**, 343–354.
12 P.-L. Kuo, H. Lee, M.-A. Bray, N. a. Geisse, Y.-T. Huang, W. J. Adams, S. P. Sheehy and K. K. Parker, *Am. J. Pathol.*, 2012, **181**, 2030–2037.
13 R. J. Jackman, D. C. Duffy, O. Cherniavskaya and G. M. Whitesides, *Langmuir*, 1999, **15**, 2973–2984.
14 E. Ostuni, R. Kane, C. Chen, D. E. Ingber and G. M. Whitesides, *Langmuir*, 2000, **16**, 7811–7819.
15 E. Kim, Y. Xia and G. M. Whitesides, *J. Am. Chem. Soc.*, 1996, **7863**, 5722–5731.
16 G. M. Whitesides, *Chem. Mater.*, 1996, 1558–1567.
17 R. Lucas, *Kolloid-Z.*, 1918, **23**, 15–22.
18 E. Washburn, *Phys. Rev.*, 1921, **17**, 273–283.
19 E. Kim and G. M. Whitesides, *J. Phys. Chem.*, 1997, **5647**, 855–863.
20 W. Huang, Q. Liu and Y. Li, *Chem. Eng. Technol.*, 2006, **29**, 716–723.
21 L. Yang, T. Yao, Y. Xu and Y. Tai, *Tech. Dig. MEMS 2002 IEEE Int. Conf. Fifteenth IEEE Int. Conf. Micro Electro Mech. Syst.*, (Cat. no. 02CH37266), 2004, vol. 14, pp. 220–225.
22 R. J. Pelham and Y. Wang, *Proc. Natl. Acad. Sci. U. S. A.*, 1997, **94**, 13661–13665.
23 D. E. Discher, P. Janmey and Y. Wang, *Science*, 2005, **310**, 1139–1143.
24 S. R. Peyton and A. J. Putnam, *J. Cell. Physiol.*, 2005, **204**, 198–209.
25 A. J. Engler, S. Sen, H. L. Sweeney and D. E. Discher, *Cell*, 2006, **126**, 677–689.
26 S. A. Ruiz and C. Chen, *Soft Matter*, 2007, **3**, 168.
27 C. Chen, J. Alonso, E. Ostuni, G. M. Whitesides and D. E. Ingber, *Biochem. Biophys. Res. Commun.*, 2003, **307**, 355–361.
28 P. Clark, P. Connolly and G. R. Moores, *J. Cell Sci.*, 1992, **292**, 287–292.
29 L. Shapiro and S. Cohen, *Biomaterials*, 1997, **18**, 583–590.
30 Y. Yamada, K. Hozumi, F. Katagiri, Y. Kikkawa and M. Nomizu, *Biopolymers*, 2010, **94**, 711–720.
31 A. Revzin, R. J. Russell, V. K. Yadavalli, W. G. Koh, C. Deister, D. D. Hile, M. B. Mellott and M. V. Pishko, *Langmuir*, 2001, **17**, 5440–5447.
32 P. Bhatnagar, A. J. Nixon, I. Kim and J. Kameoka, *Biomed. Microdevices*, 2008, **10**, 567–571.
33 Y. Aratyn-Schaus, P. W. Oakes, J. Stricker, S. P. Winter and M. L. Gardel, *J. Visualized Exp.*, 2010, 1–6.
34 J. R. Tse and A. J. Engler, *Curr. Protoc. Cell Biol.*, Wiley, 2010, Chapter 10, Unit 10.16.1–10.16.16.
35 E. Cimetta, S. Pizzato, S. Bollini, E. Serena, P. De Coppi and N. Elvassore, *Biomed. Microdevices*, 2009, **11**, 389–400.
36 J. Song, D. Tranchida and G. J. Vancso, *Macromolecules*, 2008, **41**, 6757–6762.
37 L. M. Pakstis, J. P. Dunkers, A. Zheng, T. V. Vorburger, T. P. Quinn and M. T. Cicerone, *J. Biomed. Mater. Res., Part A*, 2010, **92**, 604–614.
38 W. Brostow and J. E. Mark, *Phys. Prop. Polym. Handb.*, 2007, 423–444.
39 N. Hersch, B. Wolters, G. Dreissen, R. Springer, N. Kirchgeßner, R. Merkel and B. Hoffmann, *Biol. Open*, 2013, **2**, 351–361.
40 E. A. Cavalcanti-Adam, D. Aydin, V. C. Hirschfeld-Warneken and J. P. Spatz, *HFSP J.*, 2008, **2**, 276–285.
41 N. Hersch, B. Wolters, G. Dreissen, R. Springer, N. Kirchgessner, R. Merkel and B. Hoffmann, *Biol. Open*, 2013, **2**, 351–361.

42 T. Yeung, P. C. Georges, L. A. Flanagan, B. Marg, M. Ortiz, M. Funaki, N. Zahir, W. Ming, V. Weaver and P. A. Janmey, *Cell Motil. Cytoskeleton*, 2005, **60**, 24–34.
43 V. Damljanovic, B. Christoffer Lagerholm and K. Jacobson, *BioTechniques*, 2005, **39**, 847–851.
44 Q. Tseng, I. Wang, E. Duchemin-Pelletier, A. Azioune, N. Carpi, J. Gao, O. Filhol, M. Piel, M. Théry and M. Balland, *Lab Chip*, 2011, **11**, 2231–2240.
45 A. D. Rape, W.-H. Guo and Y.-L. Wang, *Biomaterials*, 2011, **32**, 2043–2051.
46 A. Hoffmann and P. A. Tsonis, *Springer Proceedings in Mathematics*, 2013, **15**, 7–16.
47 D.-N. Kim, J. Park and W.-G. Koh, *J. Ind. Eng. Chem.*, 2009, **15**, 124–128.
48 Y. Xia and G. Whitesides, *Annu. Rev. Mater. Sci.*, 1998, **28**, 153–184.
49 V. N. Truskett and M. P. C. Watts, *Trends Biotechnol.*, 2006, **24**, 312–317.
50 Q. Hang, Y. Wang, M. Lieberman and G. H. Bernstein, *J. Nanosci. Nanotechnol.*, 2003, **3**, 309–312.
51 K. Vats, M. Kyoung and E. Sheets, *Biochim. Biophys. Acta*, 2008, **1778**, 2461–2468.
52 S. Zhao, A. Chen, A. Revzin and T. Pan, *Lab Chip*, 2011, **11**, 224–230.
53 E. Serena, S. Zatti, E. Reghelin, A. Pasut, E. Cimetta and N. Elvassore, *Integr. Biol.*, 2010, **2**, 193–201.
54 S. Zatti, A. Zoso, E. Serena, C. Luni, E. Cimetta and N. Elvassore, *Langmuir*, 2012, **28**, 2718–2726.
55 D. Chakraborty and S. Chakraborty, in *Microfluidics and Microfabrication*, ed. S. Chakraborty, Springer, New York, 2010.
56 P. Tabeling, *Introduction to Microfluidics*, Oxford University Press, Oxford, UK, 2005.
57 V. Ganesan and H. Brenner, *Phys. Rev. Lett.*, 1998, **81**, 578–581.
58 M. Dube, M. Rost, K. R. Elder, M. Alava, S. Majaniemi and T. Ala-Nissila, *Phys. Rev. Lett.*, 1999, **83**, 1628–1631.
59 R. Planet, S. Santucci and J. Ortin, *J. Contam. Hydrol.*, 2011, **120–121**, 157–169.
60 J. Berthier, F. Loe-Mie, V.-M. Tran, S. Schoumacker, F. Mittler, G. Marchand and N. Sarrut, *J. Colloid Interface Sci.*, 2009, **338**, 296–303.
61 M. R. Nejadnik, A. L. J. Olsson, P. K. Sharma, H. C. van der Mei, W. Norde and H. J. Busscher, *Langmuir*, 2009, **25**, 6245–6249.
62 K. B. Gupta, M. B. Ratcliffe, M. a. Fallert, L. H. Edmunds and D. K. Bogen, *Circulation*, 1994, **89**, 2315–2326.
63 M. F. Berry, A. J. Engler, Y. J. Woo, T. J. Pirolli, L. T. Bish, V. Jayasankar, K. J. Morine, T. J. Gardner, D. E. Discher, H. L. Sweeney, F. Mark and J. Timothy, *Am. J. Physiol. Hear. Circ. Physiol.*, 2006, **6085**, 2196–2203.
64 H.-W. Chien, W.-H. Kuo, M.-J. Wang, S.-W. Tsai and W.-B. Tsai, *Langmuir*, 2012, **28**, 5775–5782.
65 M. L. McCain, H. Lee, Y. Aratyn-Schaus, A. G. Kléber and K. K. Parker, *Proc. Natl. Acad. Sci. U. S. A.*, 2012, **109**, 9881–9886.
66 Z. Liu, J. L. Tan, D. M. Cohen, M. T. Yang, N. J. Sniadecki, S. Alom, C. M. Nelson and C. S. Chen, *Proc. Natl. Acad. Sci. U. S. A.*, 2010, **107**, 9944–9949.
67 V. Maruthamuthu, B. Sabass, U. S. Schwarz and M. L. Gardel, *Proc. Natl. Acad. Sci. U. S. A.*, 2011, **108**, 4708–4713.
68 C. Cesa, N. Kirchgessner, D. Mayer, U. S. Schwarz, B. Hoffmann and R. Merkel, *Rev. Sci. Instrum.*, 2007, **78**, 034301.
69 D. Kirchenbüchler, S. Born, N. Kirchgeßner, S. Houben, B. Hoffmann and R. Merkel, *J. Phys.: Condens. Matter*, 2010, **22**, 194109.
70 S. Houben, N. Kirchgeßner and R. Merkel, *Proc. Ger. Assoc. Pattern Recognit. DAGM*, 2010, **6376**, 71–80.
71 C. Wohlfarth, *SpringerMaterials – The Landolt-Börnstein Database*, 2008, IV/24.
72 J. Schindelin, I. Arganda-Carreras, E. Frise, V. Kaynig, M. Longair, T. Pietzsch, S. Preibisch, C. Rueden, S. Saalfeld, B. Schmid, J.-Y. Tinevez, D. J. White, V. Hartenstein, K. Liceiri, P. Tomancak and A. Cardona, *Nat. Methods*, 2012, **9**, 676–682.
73 N. Otsu, *IEEE Trans. Syst. Man Cybern.*, 1979, **9**, 62–66.
74 P. G. de Gennes, *Rev. Mod. Phys.*, 1985, **57**, 827–863.
75 V. S. Ajaev and G. M. Homsy, *Annu. Rev. Fluid Mech.*, 2006, **38**, 277–307.
76 L. Shui, J. C. T. Eijkel and A. van den Berg, *Sens. Actuators, B*, 2007, **121**, 263–276.
77 Y. Liu, D. D. Nolte and L. J. Pyrak-Nolte, *Lab Chip*, 2012, **12**, 2858–2864.
78 D. R. Link, S. L. Anna, D. A. Weitz and H. A. Stone, *Phys. Rev. Lett.*, 2004, **92**, 54503.